Geofísica Internacional (1998), Vol. 37, Num. 3, pp. 183-199

A comparative analysis between transient electromagnetic soundings and resistivity soundings in the Tres Virgenes geothermal zone, Mexico

Carlos Flores[1] and Néctor Velasco[1,2]

[1] *Depto. de Geofísica Aplicada. División de Ciencias de la Tierra. CICESE, Baja California, México.*

[2] *Now at: Intituto Mexicano del Petróleo, Cd. del Carmen, Campeche.*

Received: September 2, 1997; accepted: March 22, 1998.

RESUMEN

Las zonas geotérmicas en áreas volcánicas están caracterizadas por relieves topográficos abruptos y resistividades superficiales variables, representadas por manantiales termales, zonas fósiles y actuales de alteración hidrotermal y la presencia de diferentes episodios de volcanismo explosivo y lávico. En este trabajo examinamos los resultados de la aplicación de sondeos electromagnéticos transitorios (TEM) de bobina central y de sondeos eléctricos verticales (SEV) en una zona geotérmica con estas características. La inversión de 62 SEV y 55 sondeos TEM da como resultado modelos estratificados promedio similares. Sin embargo, la evaluación de los modelos usando el método de descomposición en valores singulares demuestra que los sondeos TEM tienen un mayor poder resolutivo. Los factores que contribuyen al mejor desempeño del método TEM son: una mayor redundancia de datos, una mejor calidad de los datos, una menor sensibilidad a la topografía y a heterogeneidades superficiales y una menor sensibilidad a problemas de equivalencia asociados con capas conductoras delgadas.

PALABRAS CLAVE: Métodos geofísicos de exploración, sondeos electromagnéticos transitorios y de resistividad, zona geotérmica.

ABSTRACT

Geothermal zones in volcanic areas are characterized by rough topographic relief and variable shallow resistivities represented by hotsprings, modern and fossil hydrothermally altered zones, and by the presence of different episodes of lavic and explosive volcanism. We examine the performance of in-loop transient electromagnetic (TEM) and vertical electric soundings (VES) in a geothermal area with these characteristics. The inversion of 62 VES and 55 TEM soundings results in similar average stratified models. However, model assessment using the singular value decomposition method show that the TEM soundings possess a higher resolving power. Higher data redundancy, better data quality, less sensitivity to topographic and near-surface inhomogeneities, and less sensitivity to equivalence problems associated with thin conductive layers are contributing factors to the superior performance of the TEM method.

KEY WORDS: Geophysical exploration methods, transient electromagnetic and resistivity soundings, geothermal zone.

INTRODUCTION

Resistivity and electromagnetic sounding are well established methods and useful techniques for estimating the subsurface distribution of electrical resistivity. Comparisons between theoretical and field one-dimensional (1-D) responses for the transient electromagnetic (TEM) and vertical electric sounding (VES) methods (Frischknecht and Raab, 1984; Raiche *et al*., 1985; Fitterman *et al.*, 1988) have shown that the VES method is sensitive to both resistive and conductive layers; but as these layers become thin, the problem of nonuniqueness or equivalence becomes severe. The TEM method is less severely affected by equivalence in the case of conductive layers, but may also be less sensitive to layers with high resistivities.

Topographic relief and variations in the resistivity of near-surface rocks in structurally complex areas, such as geothermal zones in volcanic environments, affect the reliability of interpretation of the data in terms of layered models. The topography and local near-surface inhomogeneities distort the electric and magnetic fields of otherwise normal fields, and perturb the sounding curves. The in-loop TEM sounding method offers some advantages over the VES method when working in laterally heterogeneous areas. The smaller dimension of the TEM array is less influenced by surface topography or shallow inhomogeneities. Furthermore, the TEM data, which is based on the measurement of the derivative of the magnetic field, is less affected by these inhomogeneities, as the magnetic field is known to be less perturbed than the electric field which is measured in the VES technique.

THE SURVEY AREA

The Tres Virgenes geothermal zone is located on the eastern coast of the Baja California peninsula (Figure 1). It is related to a Plio-Quaternary volcanic complex in an active tectonic area associated with the opening of the Gulf of California. Since 1984 the Comisión Federal de Electricidad

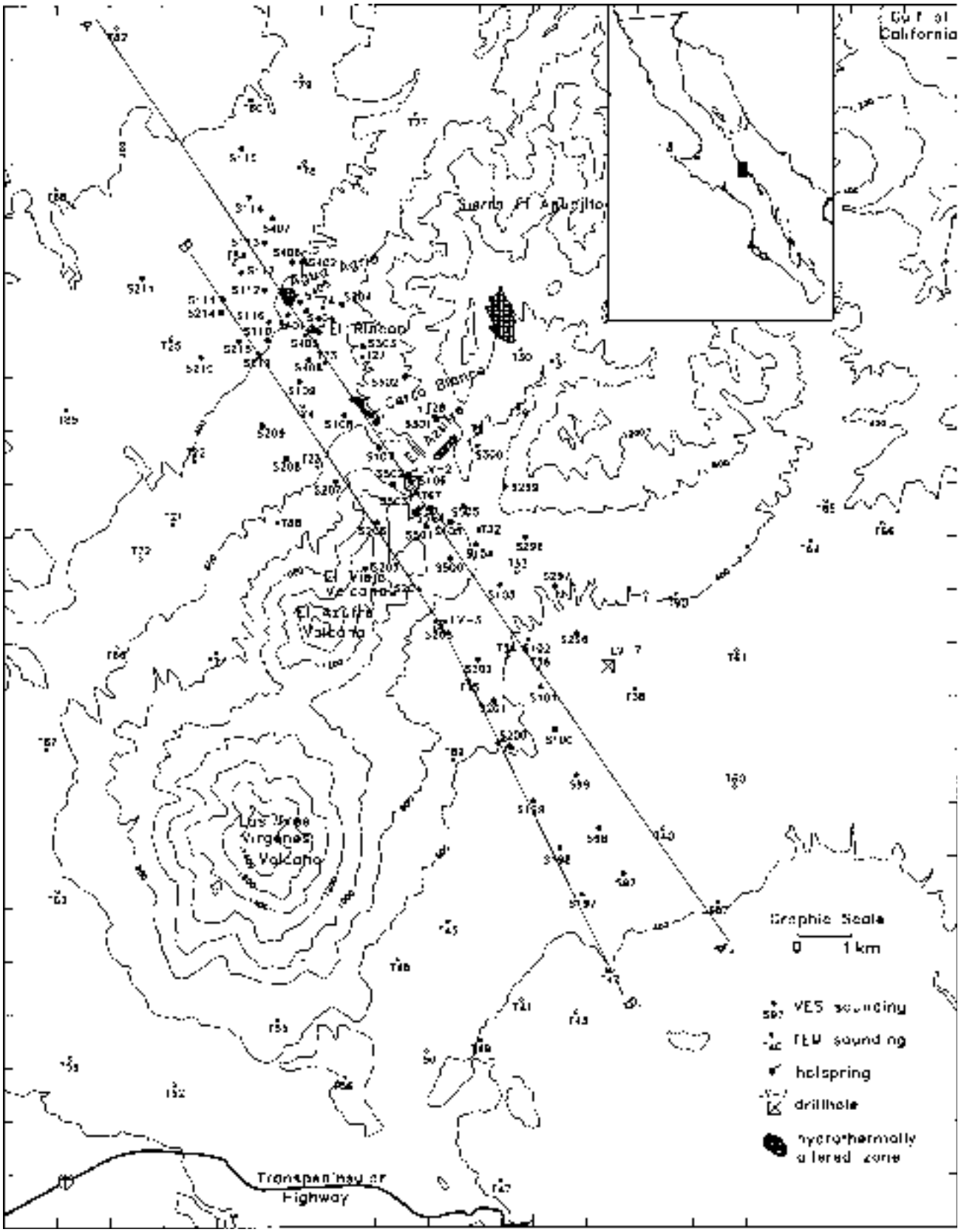

Fig. 1. Index map showing the location of the TEM and VES sites. Topographic contours every 200 m. The inset displays the location of the Tres Vírgenes area.

(CFE) has conducted intensive exploration in the area. López Hernández *et al.* (1994, 1995) summarize the geological, geophysical, and geochemical studies, and the results of the exploratory drilling. The lithologic column of the area, obtained from the drillholes, is as follows: at the base of the sequence a Cretaceous granodioritic basement, associated with the Baja California batholith, is found at depths of 900 - 1000 m. In this unit temperatures in excess of 220°C have been measured, where fluids of magmatic origin occur in low-permeability rocks. This basement is overlain by the Comondú Group, a volcano-sedimentary sequence of Late Oligocene - Middle Miocene age, with a maximum thickness of 750 m; the Santa Lucía andesites form the upper part of this sequence. Shallow marine sediments of the Santa Rosalía basin rest on the Comondú Group, followed by volcanic rocks of Plio-Quaternary age. These came mainly from three eruptive centers. They are, in chronological order, La Reforma, a resurgent calderic structure located east of the study area; the Sierra El Aguajito; and the Tres Vírgenes volcanic complex, which is formed by three N-S aligned composite volcanoes showing progressively younger ages to the south. The last volcanic activity in the Tres Vírgenes edifice was reported in 1746 by Spanish explorers.

In 1994 a magnetotelluric (MT) survey, consisting of 90 sounding sites, was completed (Vázquez *et al*., 1992; Romo *et al*., 1994). In this study 55 TEM sites were also measured, with the original purpose of applying the static shift correction to the MT data. The large amount of TEM sites and the similar depths of penetration of these data with those of 62 VES sites, previously acquired by CFE, provides an opportunity to compare the data in terms of the degree of distortion produced by near-surface inhomogeneities and topography and to analyse how this affects the resolution of the interpreted layered models.

THE DATA

Transient EM soundings in the central or in-loop configuration are made with a large rectangular or square transmitting loop and a horizontal receiving coil located at the center of the loop . The injected dc current in the loop is periodically interrupted in the form of a linear ramp. An induced current system, flowing in closed paths below the loop and created each time the transmitter current is interrupted, produces a secondary magnetic field. The time variation of the vertical component of this magnetic field induces a voltage in the receiver coil. As the spatial and temporal distribution of the subsurface current system depends upon the ground resistivity, the measured transient voltage gives information about the subsurface resistivity. The locus of the maximum amplitude of the induced currents diffuses downward and outward with time, thereby giving information about deeper regions as time increases (Nabighian, 1979; Hoversten and Morrison, 1982).

The location of the 55 TEM sounding sites is shown in Figure 1 . They were acquired with a Geonics TEM57 system, employing 150 m square loops in most of the sites and measuring the transient voltages with a multi-turn receiver coil arranged in the in-loop configuration. Three repetition frequencies (30, 7.5, and 3 Hz) of the bipolar current waveform were used, injecting currents of 7.5 A. The transient voltages were measured in 20 time windows for each repetition frequency, resulting in transient curves composed of 60 partially overlapping records ranging from .09 to 70 ms. Ten transient decays were recorded for each repetition frequency, each decay representing the average of 50 to 500 individual measurements. Nearby lightning represented the main source of electromagnetic noise particularly in a couple of sites. Data editing consisted in neglecting saturated decays and negative voltages occurring in the late-time windows. Negative voltages can be produced by a number of sources (Spies and Frischknecht, 1991; Nabighian and Macnae, 1991); for the in-loop array in this geologic environment the most probable candidate is the presence of a frequency-dependent conductivity giving rise to induced polarization (IP) (Smith and West, 1989). Although an IP effect can not be ruled out as a possible source of contamination of our data, we favour low signal/noise ratios to explain negative voltages, as they occur in the late-time windows where the voltages fall within the estimated summer noise level of 1 to 10 nV/m^2 (Spies, 1989; Fitterman, 1989). Furthermore, most of the negative voltages tend to occur in a few soundings where the transmitter moment was smaller and in a group of eight soundings located over a more resistive subsurface structure (confirmed by the nearby VES models).

The stacked transient voltages were transformed to late-time apparent resistivity curves as a function of time (Kaufman and Keller, 1983). Figure 2a shows the late-time apparent resistivity curves for the worst and best cases (soundings T40 and T33), using as the quality measure the root-mean-squared (rms) misfit error, defined as

$$\varepsilon = \left[\frac{1}{M-N} \sum_{i=1}^{M} \left(\frac{d_i - c_i}{d_i} \right)^2 \right]^{1/2} \times 100\% \qquad (1)$$

where d_i are the M observed data, c_i are the M calculated apparent resistivities from the best-fitting layered model (to be discussed below), and N is the number of model parameters.

The VES data were acquired by CFE in different field surveys starting in 1983 (Ballina and Herrera, 1985; Bigurra, 1989). The 62 Schlumberger sites do not cover the same area of the TEM soundings, but are concentrated along a NW-SE corridor (Figure 1). Typically, the current electrode separations (AB/2) varied from 10 m up to 3 km, giving seven apparent resistivity values per decade. These data were acquired following the standard field procedure for the Schlumberger array, namely, the gradual increase in steps of

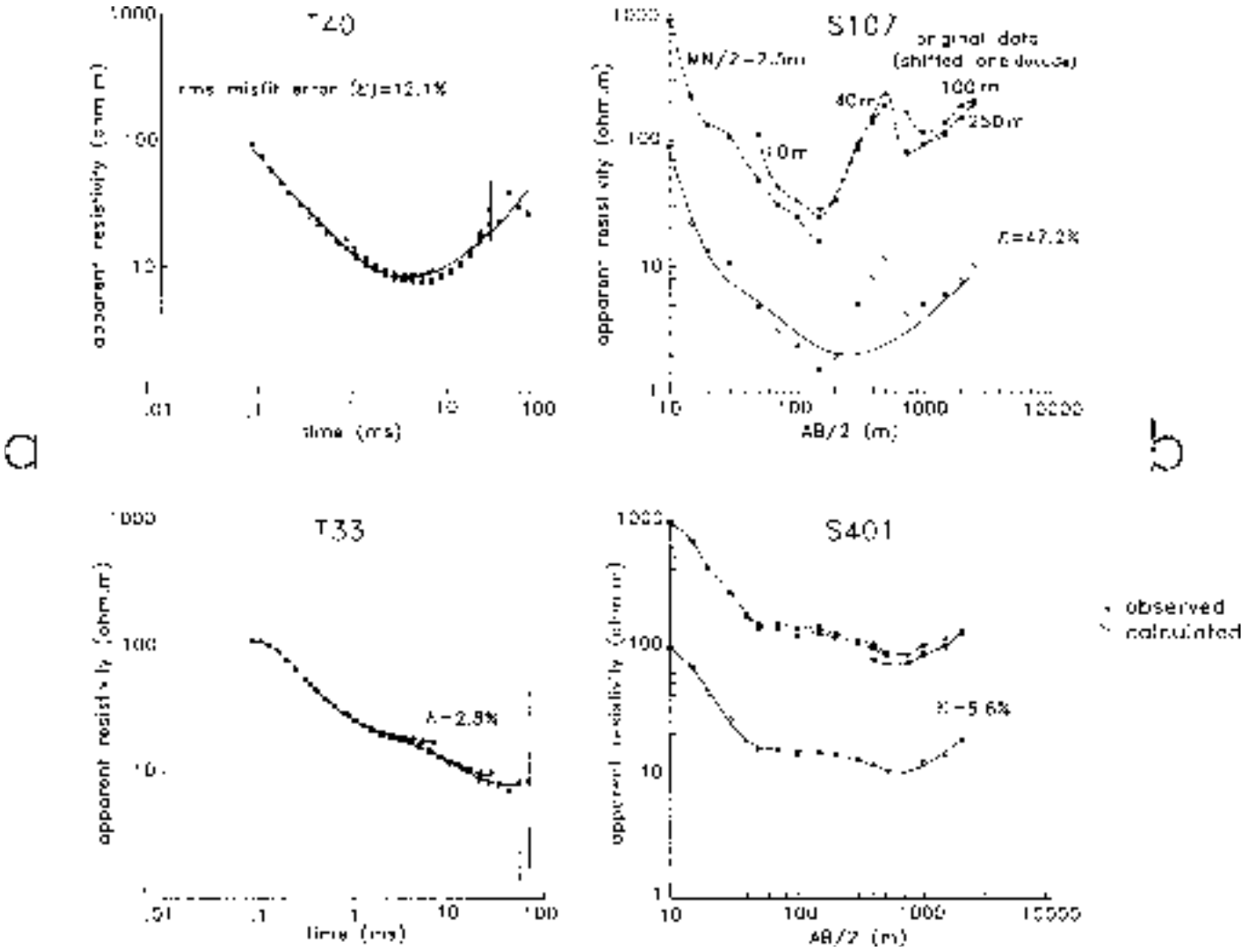

Fig. 2. Worst and best sounding data in terms of the root mean squared (rms) misfit error. a) TEM soundings T40 and T35. Error bars are +/- one standard deviation. b) VES soundings S107 and S401. Original apparent resistivity data are shifted up one logarithmic decade. MN/2 stands for half the potential-electrode separation.

the potential electrode spread (MN/2) as the current electrode separation increases. Typical values of MN/2 varied from 2.5 m up to 250 m.

Figure 2b shows the VES apparent resistivity data for the worst and best soundings, where the data quality is also measured in terms of the rms misfit error. The original data for the sounding S107 (shifted upward one decade for clarity) illustrate the typical noise problems in the Schlumberger data. The symbols connected by dashed lines define segments of apparent resistivities obtained with the same potential electrode spread. Strong vertical shifts between the different segments, especially between the segments of MN/2=2.5 m and 10 m, are evident. These shifts are the result of charge distributions built up at the boundaries of local resistivity inhomogeneities located in the vicinity of one or both potential electrodes. These electric charge distributions enhance or depress the otherwise normal electric field of the layered ground. This perturbing effect is known in the practice of magnetotelluric soundings as the static shift effect (Jones, 1983; Jiracek, 1990). The presence of these inhomogeneities does not only affect the measured potential in the potential electrodes but also perturbs the geometry and intensity of the current flow set up by the current electrodes. This effect is evident in the local maximum peaking at AB/2=500 m in sounding S107, having slopes too strong as to be reproduced by any layered model.

In order to correct the shifts between the different segments some interpreters prefer to maintain fixed the segment of large potential-electrode separation and vertically displace the segments of shorter separations to obtain a continuous curve, while others choose to fix the short or an intermediate-separation segment. Any of these approaches is valid as long as the interpreter has a priori knowledge of where the near-surface inhomogeneities are located relative

to the center of the spread. We systematically fixed the shortest spread and moved up or down the segments for larger potential electrode separations in the log-log graphs. In order to incorporate uncertainties to the data resulting from this correction we calculated the average vertical shift for all soundings, resulting in a value of 32.3% of the apparent resistivities. This value was assigned as a global error to all the apparent resistivity data employed in the inversion process, except in the comparative case below, where the errors were estimated individually for each Schlumberger sounding.

DATA INVERSION

The TEM late-time apparent resisistivity data at each site were inverted to a layered model using the Temixgl software package developed by Interpex Ltd. The inversion is performed using a ridge regression algorithm (Inman, 1975) to iteratively adjust the parameters of a starting model until a model is obtained which best fits the data in the least squares sense. The solution to the forward problem required in each iteration is calculated using the digital linear filters designed by Anderson (1975; 1979). An equivalent dipole approximation (Stoyer, 1990) is adopted to consider square or rectangular loops. The effect of the linear ramp is accounted for by convolving the ramp with the step turn-off response, as described by Fitterman and Anderson (1987).

The Schlumberger apparent resistivity data were also inverted to layered models. In this case the linearized inversion algorithm described by Jupp and Vozoff (1975) was used.

MODELING RESULTS

Both the TEM and VES data were inverted to the minimum number of layers which best reproduced the data. The resulting TEM models consisted of 3, 4, 5 and 6 layers, with the major contribution coming from the four-layered models (65% of the models). The calculated data from the inverted models reproduced well the observed data as measured by the rms misfits. The average and standard deviation of the misfits were 5.8% and 1.9%, respectively. The distribution of these errors is shown in Figure 3.

Most of the models feature one or several conductive layers overlain by one or more resistive layers and underlain by a resistive substratum. We transformed all the models into a simplified H-type model ($\rho_1 > \rho_2 < \rho_3$) using the equivalent transverse resistance (T) for the group of shallow resistive units and the equivalent longitudinal conductance (S) for the conductive layers. Let us denote the parameters of the three layers of these simplified models by the subscripts R, C, and B, for resistive, conductive, and basement, respectively. From the global behavior of the TEM and VES models, we assigned a conductive layer to the conductive equivalent layer if its resistivity had a value less than 50 Ωm.

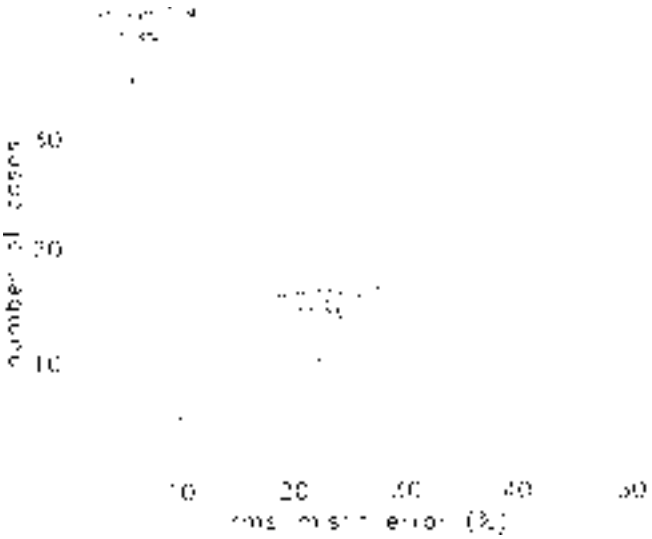

Fig. 3. Distribution of rms misfit errors for the TEM and VES soundings.

Figure 4 shows the average H-type TEM model with error bars (+/- one standard deviation) for the layer resistivities and thicknesses. Standard deviations are defined in the logarithmic space and are reported as percentages of a decade. Table 1 displays the average, standard deviation, maximum and minimum values found for each equivalent layer. The R layer is composed mainly by one or two layers. The resistivity (ρ_R) of this unit has an average value of 181 Ω·m but shows a high dispersion as evidenced by their standard deviation (38% of a decade) and maximum value (1861 Ω·m). The thickness (t_R) of this layer also shows a high variability. The average, standard deviation, and maximum values are 107, 29%, and 462 m, respectively. No minimum values for ρ_R and t_R are reported because in four of the models, located close to the hydrothermal zones, the shallowest layer resulted with values less than 50 Ω·m. The C layer is composed mostly by two layers. In contrast to the R layer, it shows a smaller dispersion. Their average equivalent resistivity (ρ_C) and thickness (t_C) are 4.75 Ω·m and 331 m, respectively, with standard deviations of 27% and 26%.

The basement resistivity (ρ_B) is not a well resolved parameter. The apparent resistivities at the latest times (typically times greater than 20 ms) are those contributing more to the estimation of ρ_B. These values are particularly contaminated by noise as the measured voltages are below or close to the 1 to 10 nV/m^2 noise level (Fitterman, 1989). At four sites the apparent resistivity curve did not show the ascending branch characteristic of sensing a resistive layer. In these cases the reported value for ρ_B was based on the behavior of neighbouring sites where the ascending branch was evident. In 64% of the models the reported ρ_B represents a lower bound, i.e., larger values are possible in the sense that their calculated responses fit the observed data with comparable misfit.

Table 1

Statistical parameters of the average H-type simplified models. Standard deviations are expressed as percentages of a logarithmic decade

	TEM				VES			
	average	standard deviation	maximum	minimum	average	standard deviation	maximum	minimum
rms error	5.8%	1.9%	12.1%	2.8%	22.2%	9.9%	47.2%	5.8%
ρ_R	181 Ω·m	38%	1861 Ω·m		332 Ω·m	51%	9300 Ω·m	
t_R	107 m	29%	462 m	—	64 m	50%	420 m	—
ρ_C	4.75 Ω·m	27%	15 Ω·m	1.22 Ω·m	2.65 Ω·m	33%	13.5 Ω·m	0.36 Ω·m
t_C	331 m	26%	884 m	93 m	387 m	16%	807 m	127 m
ρ_B	84.7 Ω·m	58%	1189 Ω·m		46.8 Ω·m	36%	298 Ω·m	7.44 Ω·m

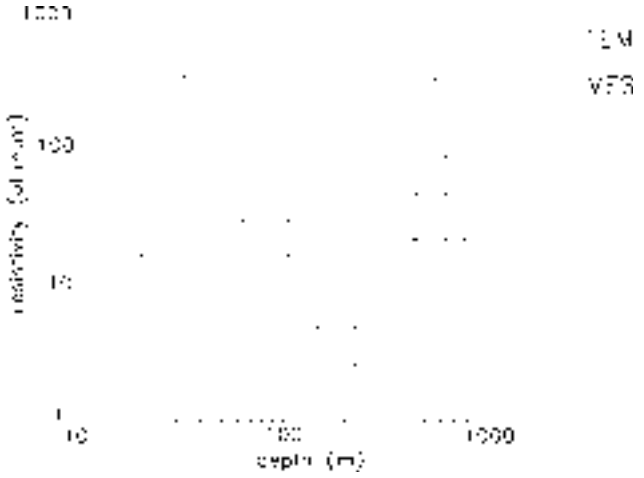

Fig. 4. Average simplified H-type models. Error bars are +/- one standard deviation.

Different subsets of the VES data were interpreted by Ballina and Herrera (1985) and Bigurra (1989) using the curve-matching technique of Orellana and Mooney (1966) and by Vázquez *et al.* (1992) employing an inversion approach. Our initial inversions of selected soundings showed significant differences with previous models. Thus decided to reinterpret the whole VES data set. These discrepancies can be explained by the non-uniqueness of the inversion problem, the limited number of models available in the Orellana and Mooney set, the errors in the visual interpolation procedure inherent in the curve-matching technique, equivalence problems in the models, and the large scatter and errors in the apparent resistivity data. The latter factor has an important effect on the reliability of these models. In many instances the inverted models did not correlate well with neighbouring TEM and VES models. These discrepancies were somewhat reduced by employing, in the inversion process, initial models based on the depths to layer interfaces of nearby TEM models.

Most of the VES models consist of four and five layers. The general behavior of the models agrees with that obtained from the TEM data, showing a group of resistive layers underlain by one or two conductive layers and a resistive basement sensed by the longest array separations. However, the rms misfit errors were significantly larger than those of the TEM models. The average error is 22.2% compared to the average TEM error of 5.8% (Table 1 and Figure 3). The main contribution to the large VES error comes from the difficulty on fitting the strong slopes surrounding the apparent resistivity minima.

As in the TEM models, we synthetized the VES models into H-type simplified models using equivalent parameters. The resistivity and thicknesses of the R layer show a high variability, with average values of 332 Ω·m and 64 m (Figure 4 and Table 1). This layer is absent in only three sites where the resistivities of the shallow layers fall below the 50 Ω·m value. These sites (S403, S404 and S503) occur close to the hotsprings. The conductive C layer is mainly composed by one or two layers, with average equivalent resistivity of 2.65 Ω·m and thickness of 387 m. The electric basement has a mean value of 47 Ω·m.

Sections A-A' and B-B'of Figure 1 are shown in Figures 5 and 6; they include a total of 14 TEM and 44 VES soundings. For reasons of space each section is split into two

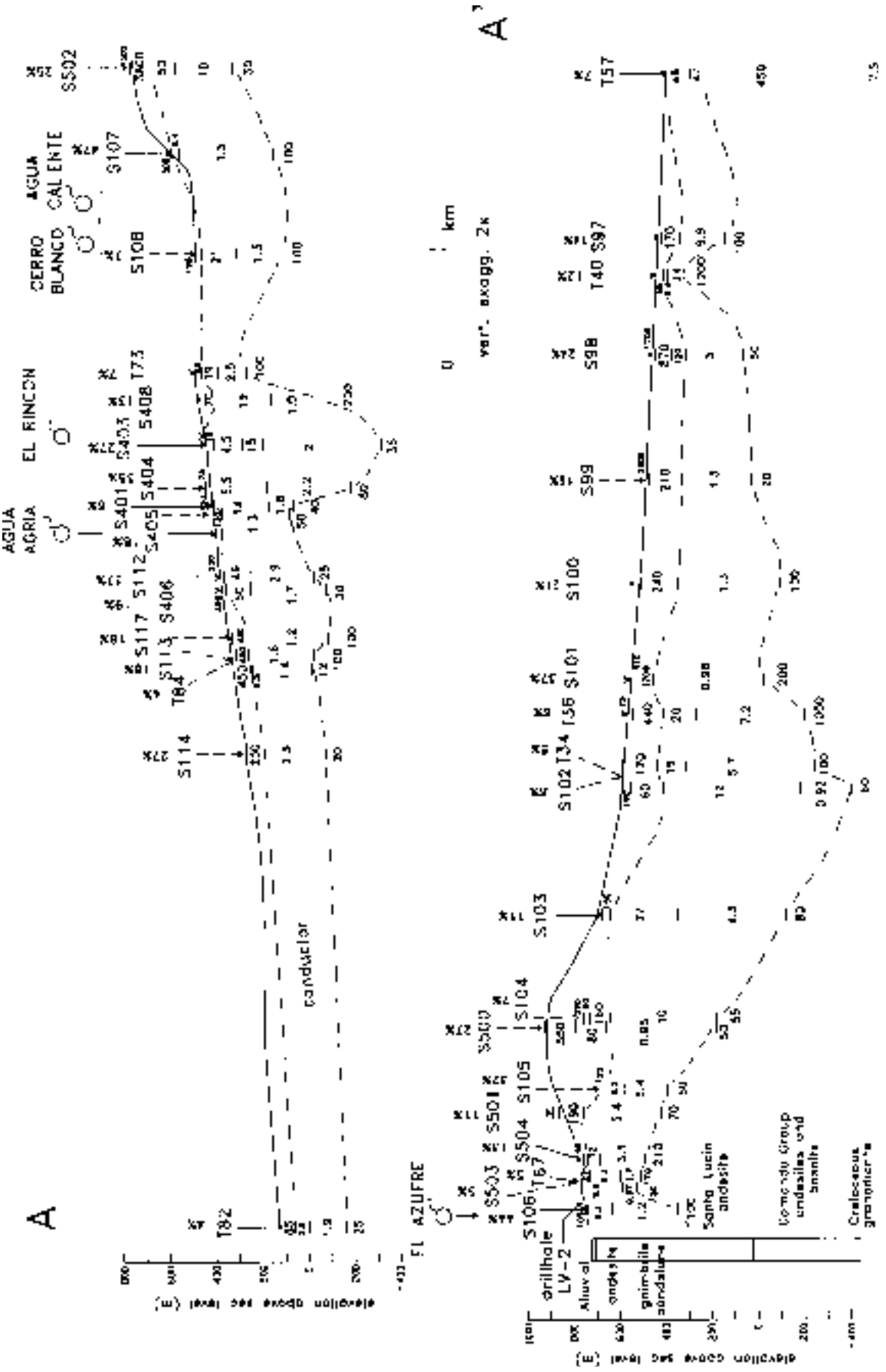

Fig. 5. Geoelectric section A-A'. The lower panel is the continuation of the upper panel. Dashed vertical lines indicate sites more than 200 m off the line of section. Dashed horizontal lines enclose the conductive layer of the simplified model. Values under each site are the modeled resistivities in ohm.m. Percentage values above each sounding denote the rms misfit errors.

parts. The location of the soundings is shown with arrows, using dashed arrows when the site is more than 200 m off the section. The layer interfaces and resistivities of the inverted models are displayed under each site. We include, above each site, the rms misfit error. The lithologies encountered in drillholes LV-2 and LV-3 and the location of the hotsprings are also indicated. The dashed lines display the proposed correlations of interfaces which define the top and bottom of the conductor discussed above. This unit is interpreted as being the electrical expression of the regional aquifer. The depth to the top of this conductive unit tends to be shallow and it outcrops in the vicinity of the hotsprings and hydrothermal zones. In these zones the thickness of the conductor shows abrupt variations which may be a combined effect of near-surface resistivity variations and feeding zones of hot water at depth. The depths of exploration of both TEM and VES soundings do not reach depths greater than 1 km, where drillhole temperatures in excess of 220˚C suggest the presence of a geothermal reservoir. Further interpretations of the electric structure in terms of geological and geothermal features are beyond the scope of this work and will be published elsewhere.

MODEL ASSESSMENT

Model assessment is carried out in two steps. First, the technique of Edwards *et al*. (1981) is used to define which model parameters or combination of parameters are well resolved and which are not. Second, the errors in the parameters are estimated by using the approach of Raiche *et al*. (1985). Both techniques are based on the singular value decomposition (SVD) of the sensitivity matrix. Before going into the analysis of the inverted models, a brief account of these methods is given.

Consider a stratified model with parameters p_j, $j = 1, N$. These parameters are the layer thicknesses and resistivities. Each datum or apparent resistivity measured at the surface of the earth is denoted by y_i, $i = 1, M$ ($M > N$), each having a standard error e_i. By linearization, the expected changes in the data dy_i, produced by small variations dp_j in the parameters, are given by

$$dy_i = \sum_{j=1}^{N} A_{ij} dp_j \quad i = 1, M \quad ,$$

or in matrix notation, $d\mathbf{y} = \mathbf{A}\, d\mathbf{p}$, (2)

where each coefficient A_{ij} is the partial derivative $\partial y_i / \partial p_j$, i.e., is a measure of how sensitive is the datum y_i to a change in the parameter p_j.

The sensitivity matrix **A** is decomposed using the SVD technique, giving

$$\mathbf{A} = \mathbf{U}\ \mathbf{S}\ \mathbf{V}^T, \qquad (3)$$

where T stands for transpose, **U** (M x N) and **V** (N x N) are the eigendata and eigenparameter matrices, and **S** (N x N) is a diagonal matrix containing the singular values or eigenvalues.

Edwards *et al*. (1981) showed that if the coefficients of the sensitivity matrix are normalized by the data errors e_i, then the errors in the eigenparameters, defined by

$$d\mathbf{p}^* = \mathbf{V}^T d\,\mathbf{p} \ , \qquad (4)$$

are $1/s_{jj}$, the reciprocal of the corresponding eigenvalue.

Besides dividing each element of matrix **A** by e_i, they are also multiplied by p_j, which has the effect of redefining the p_j as the logarithms of the model parameters rather than the parameters themselves. This scaling facilitates the physical interpretation of the eigenparameters as will be shown in an example below. The coefficients of the matrix **A** were estimated here by forward differences perturbing 5% the model parameters.

The error bounds for the model parameters (Raiche *et al*., 1985), are given by

$$p_j^{\pm} = p_j \exp(\pm B_j \beta) \ , \qquad (5)$$

with

$$B_j = \left[\sum_{k=1}^{N} \left(\frac{V_{jk}}{s_k} \right)^2 \right]^{\frac{1}{2}} \ , \qquad (6)$$

and

$$\beta = \left[\frac{1}{M-N} \sum_{i=1}^{M} \left(\ln\left(\frac{d_i}{c_i} \right) \right)^2 \right]^{\frac{1}{2}} \ , \qquad (7)$$

where $p_j^{\pm}$ are the upper and lower bounds of a 68% confidence level for the parameter p_j, V_{jk} are the coefficients of the eigenparameter matrix **V**, s_k are the eigenvalues, d_i are the observed data and c_i the calculated data from the layered model. Expression (7) for β is a logarithmic version of (1), the rms misfit error between observed and calculated responses. The exponential in (5) takes into account the logarithmic definition of both the parameters and the misfit error.

Equation (5) includes the different factors contributing to the reliability of the model, namely: a) the statistics of the data through the number of data M and the normalization of the sensitivity matrix by the data errors e_i, b) the physics of the problem and the sensitivity of the available measurements to the parameters through the sensitivity matrix, and c) the level of fit through expression (7).

Figure 7 illustrates the two-step procedure of model assessment and introduces the particular format adopted in the application to actual field models. The data (Figure 7a) consist of seven Schlumberger apparent resistivity values

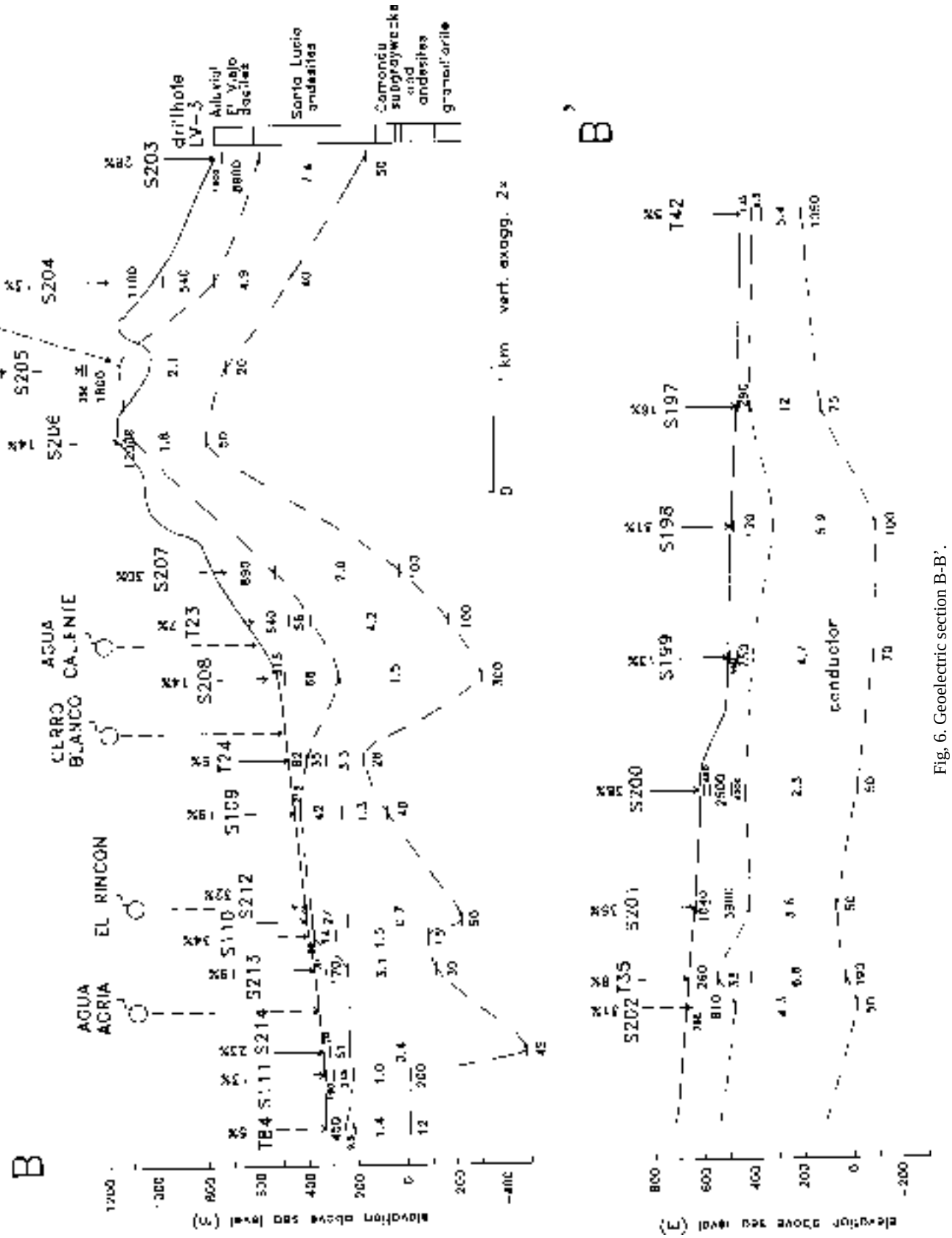

Fig, 6. Geoelectric section B-B'.

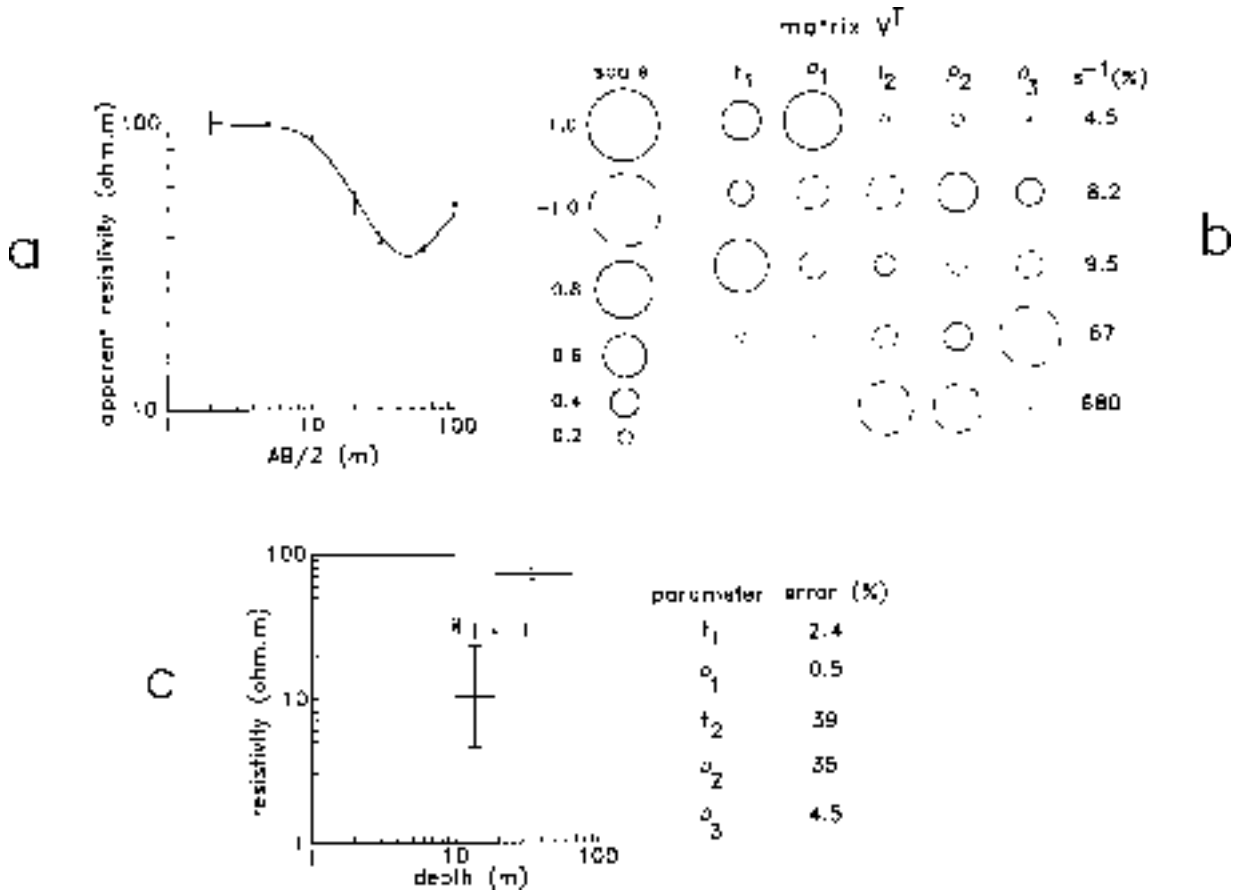

Fig. 7. Assessment of the Schlumberger synthetic model. a) Apparent resistivity values with 10% data errors. The calculated response from model in c) is shown with solid line. b) Coefficients of the transposed eigenparameter matrix. The size of the circles is proportional to the coefficients according to the displayed scale. Dashed circles indicate negative coefficients. Standard errors are indicated in the rightmost column. c) Model and error bars. The error values are expressed as a percentage of a decade.

calculated from a three-layer model characterized by having a thin and conductive second layer. This case is designed to show how the assessment procedure detects and quantifies the S-equivalence problem of this model. A 10% error is assigned to these synthetic data. The model to be analysed is shown in Figure 7c, its calculated response being plotted in Figure 7a with a continuous line. Figure 7b displays graphically the coefficients of $\mathbf{V}^T$, the transpose of the eigenparameter matrix. The size of the circles is proportional to the coefficient values according to the displayed scale, using dashed circles for negative coefficients. As there are five parameters (two thicknesses and three resistivities) in this model, $\mathbf{V}^T$ is a 5 x 5 matrix. Each row corresponds to one eigenparameter as defined by expression (4), being arranged in order of increasing standard error. These errors, expressed in percentages, are the reciprocal of the corresponding eigenvalues and are shown in the rightmost column of Figure 7b. We will discuss the second and fifth rows, the eigenparameters containing more information on the parameters of the second layer (t_2 and ρ_2). The second eigenparameter, with a standard error of 8.2%, represents

$$dp_2^* = .35d(\ln t_1) - .45d(\ln \rho_1) - .49d(\ln t_2) + .54d(\ln \rho_2) + .37d(\ln \rho_3)\ .$$

This linear combination of the logarithmic parameters has as the most important coefficients those associated with $\ln t_2$ and $\ln \rho_2$; these coefficients (-0.49 and 0.54) have about the same magnitude but are of opposite signs. Neglecting the smaller coefficients, the combination can be approximated as $-0.49d(\ln t_2) + 0.54d(\ln \rho_2) \cong -0.52d(\ln t_2 \sigma_2)$, which can be interpreted physically as stating that the conductivity-thickness product (conductance S) of the second layer is fairly well resolved because the standard error is 8.2%.

The fifth row of Figure 7b is the linear combination

$$dp_5^* = .04d(\ln t_1) + 4\times10^{-4} d(\ln \rho_1)$$
$$-.74d(\ln t_2) - .67d(\ln \rho_2) - .02d(\ln \rho_3)\ .$$

Neglecting again the terms with small coefficients, it can be approximated by

$$-.74d(\ln t_2) - .67d(\ln \rho_2) \cong -.7d(\ln t_2 \rho_2)\ .$$

This combination of parameters means that the resistivity-thickness product (resistance T) of the second layer is not resolved at all due to the large standard error of 680%. As the conductance (t_2/ρ_2) of this layer is fairly well resolved but not so the resistance ($t_2\ \rho_2$), the thickness and resistivity cannot be separately resolved.

The errors in the five parameters are shown as error bars in a log-log scale and as percentage values of a logarithmic cycle (decade) in the right portion of Figure 7c. For this case a slight modification of equation (5) was used. As the misfit errors (d_i - c_i) are smaller than the data errors e_i, d_i / c_i in the definition of the rms logarithmic misfit error β (equation (7)) was replaced by (c_i + 0.1 d_i) /c_i, where the factor 0.1 corresponds to the 10% error assigned to the synthetic data. This correction to the rms misfit error attempts to avoid overfitting the data, that is, fitting the data to a lower level than allowed by the data errors. Returning to Figure 7c, the parameter errors reflect the information contained in the eigenparameters. The best resolved parameter is ρ_1 with an error of 0.5%, reflecting the fact that the main coefficients of ρ_1 are in the three first rows of Figure 7b. The worst resolved parameters are t_2 and ρ_2, with errors of 39% and 35% respectively, which is the result of the S-equivalence affecting this model.

COMPARATIVE CASE

Several cases were constructed by comparing VES and TEM models of nearby soundings. In order to refer the models to geologic information we selected one case which had a drillhole in the close vicinity of the soundings. The conclusions drawn from this case are similar to those from the cases not included here.

This case includes two Schlumberger soundings (S106 and S503), one TEM site (T67), and drillhole LV-2. Figure 8a shows the location of the three sites, the drillhole, and a nearby hotspring surrounded by a halo of hydrothermally altered rocks. The section of Figure 8b displays the lithologies encountered in the hole and the inverted layer resistivities under the three sounding sites. The models under sites T67 and S503 consist of four layers while that under S106 is of five layers. Dashed lines indicate proposed correlations between the layer interfaces and the geologic contacts. Correlations are good between the layer resistivities and depths to interfaces under T67 and S503 with the different geologic units found in the hole. However, lateral correlations with the model under S106 are not clear.

Figure 8c displays the observed data with error bars (+/- one standard deviation) and the calculated responses for the three soundings. The data errors for early and intermediate times for T67 are too small to be seen on this scale. As before, the original apparent resistivity data (without shift correction) for the two VES soundings are shown displaced upward one decade. The data for S106 show strong vertical shifts between the various apparent resistivity segments and intense variations within some segments. The electrode spread was along a NW-SE direction. This noise can be explained by the passage of the different electrodes close to the hotspring and over the hydrothermally altered zone (see Figure 8a) where abrupt spatial variations of the ground resistivity are expected. The calculated response of S106 poorly fits the observed data (rms misfit error of 44%), being only a smooth version of the data, especially between AB/2 values of 70 m and 750 m. It is not surprising that the final model for this sounding (Figure 8b) does not correlate well with the geologic interfaces in the drillhole. The apparent correlation of the interface between the 1.2 and 100 $\Omega \cdot m$ layers with the base of the fossiliferous sandstone may be a coincidence.

The different segments of sounding S503 show vertical shifts of lower intensity and smaller variations within the segments compared to those of S106. In this sounding the electrode spread was also laid down along a NW-SE direction, but it did not cross the alteration zone, which explains the smaller effect of shallow inhomogeneities on the data. The agreements between observed and calculated responses for T67 and S503 are good, with comparable rms errors of 5.3% and 4.5%, respectively.

The two panels of Figure 8d display the coefficients of the $\mathbf{V}^T$ matrix for the four-layer models T67 and S503. We do not include the corresponding matrix for S106 because of its poor fit with the observed data. The different linear combinations of logarithmic parameters for both models are quite complicated and will not be discussed. Instead, as both models contain a conductive layer which might pose S-equivalence problems, we examine those rows containing major contributions from the thickness (t_3) and resistivity (ρ_3) of the third layer. In the T67 model ρ_3 and t_3 appear separately in the fifth and sixth rows with standard errors of 0.48% and 1.4%, respectively. In the S503 matrix these parameters occur in pairs, in the second row where the corresponding coefficients have opposite signs and the eigenparameter has a standard error of 4.9%, and in the last row where they appear with the same sign and the combination has an error of 154%. These features indicate that the thickness and resistivity of this conductive layer are well resolved by the T67 data because the associated coefficients occur separately in two rows (fifth and sixth), both having small errors (0.48% and 1.4%). The conductance of this layer is well resolved by the VES data because the weights occur with opposite signs in a row with low error (4.9%) but the thickness and resistivity are not separately resolved because the resistance occurs in a linear combination with a very large error of 154%. Therefore, the model inverted from the TEM data is not affected by equivalence but the corresponding model derived from the VES data is affected.

Figure 9a displays the corresponding models in a log-log scale and the error bars (+/- one standard deviation) calculated from expression (5). The error bars with ending ar-

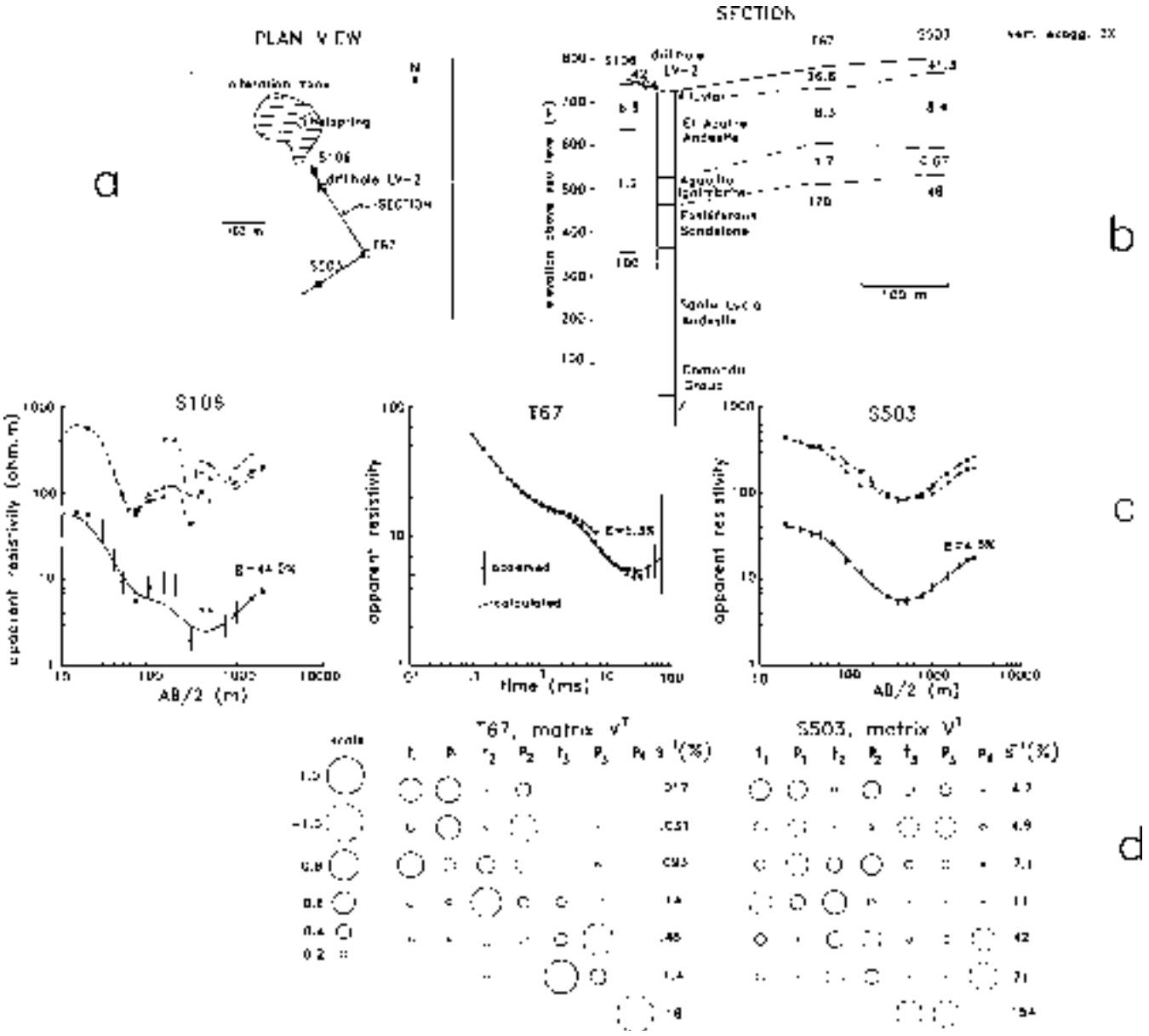

Fig. 8. Comparative Case. a) Plan view of the sounding sites, drillhole, the Los Azufres hotspring, and alteration zone. The location of the cross-section is also shown. b) Geoelectric section with the modeled interfaces between layers and resistivities. Lithologic column found in drillhole LV-2. Dashed lines denote the proposed correlations between electric layers and geologic units. c) Observed and calculated apparent resistivities for soundings S106, T67, and S503. The original Schlumberger data are plotted with a vertical displacement of one decade. The dashed lines define the different apparent resistivity segments (data with the same potential-electrode spread). Error bars are +/- one standard deviation. The rms misfit error (ε) for each sounding is also shown. d) Coefficients of the transposed eigenparameter matrices for the T67 and S503 models.

rows indicate error bounds falling off the plotted scale. The large errors in t_3 and ρ_3 for the S503 model reflect the S-equivalence problem affecting the VES model discussed above. Note the extremely low errors in the parameters of the T67 model. Even the worst resolved parameter (ρ_4) of the TEM model has an error (1%) of comparable magnitude to that of the best resolved parameter of the VES model (ρ_1 with a 0.6% error). In the following, a critical analysis is performed to evaluate the different factors contributing to the apparent superiority of the TEM method.

In general, three factors influence the degree of resolution of a given layered model. First, the amount of information from which the model is derived, i.e. the data redundancy expressed as the number of data and the data density. The TEM sounding has a higher data redundancy than the

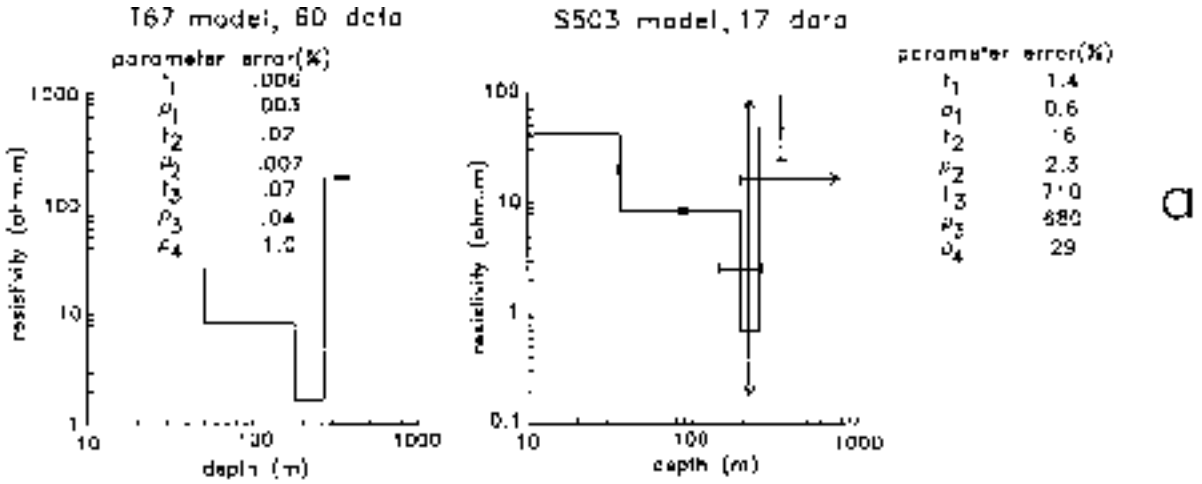

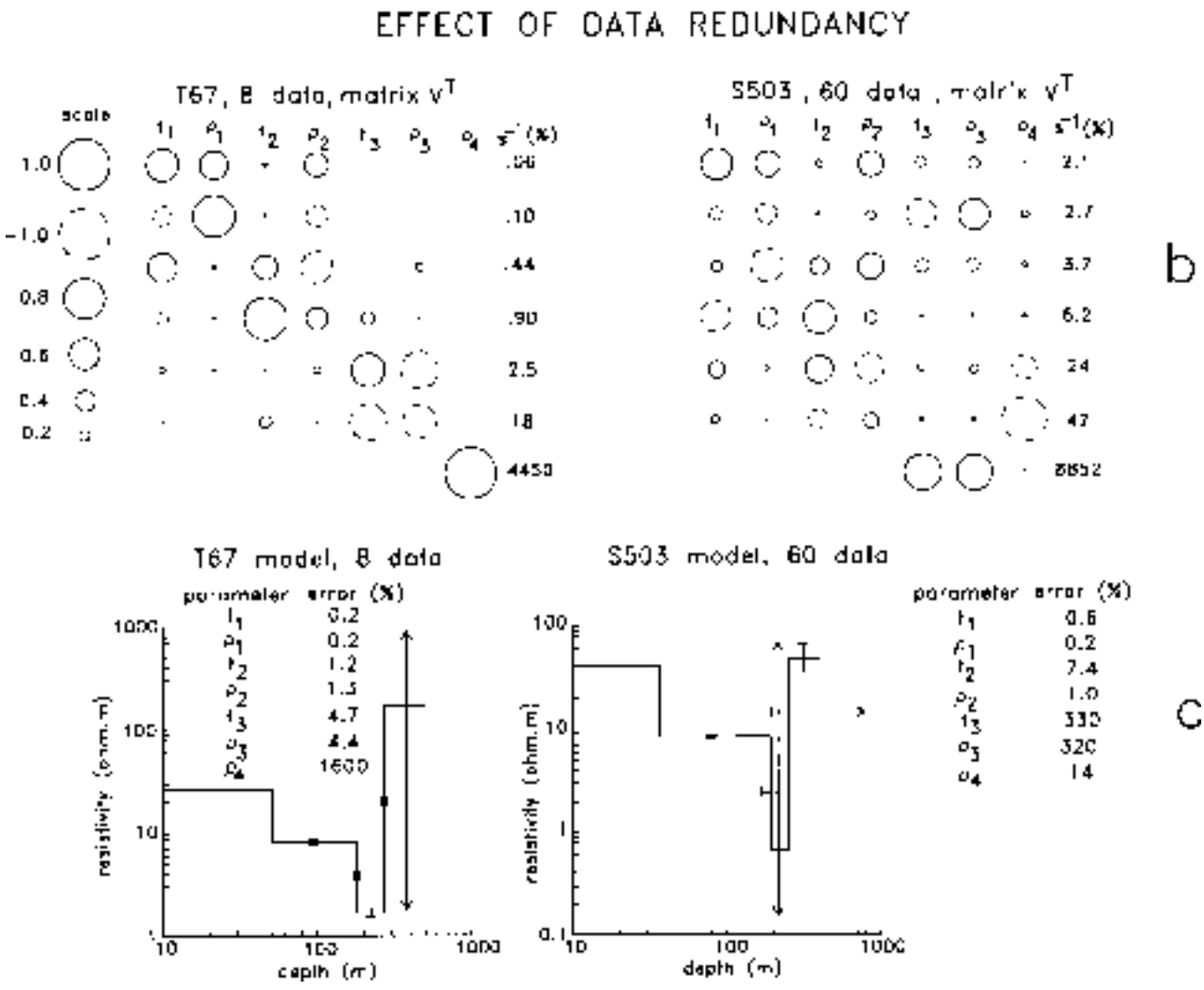

Fig. 9. a) Models and parameter errors for soundings T67 and S503 of the Comparative Case. Ending arrows in error bars indicate error bounds falling off the plotted scale. b) and c) Data redundancy analysis for the Comparative Case. The number of data for the T67 sounding is reduced to 8, for the S503 sounding is increased to 60. b) Transposed eigenparameter matrices. c) Models and parameter errors.

Schlumberger sounding. It consists of 60 data with as high as 29 data points per decade, while the VES sounding has 17 data with a uniform data density of 7 points per decade. The second factor is the data dispersion, indirectly measured by the rms misfit error, and the uncertainties in the data expressed as data errors. The rms misfit errors are comparable in magnitude for the two models, but the TEM sounding has smaller data errors. The distribution of the T67 data errors is not homogeneous; in 48 out of 60 data the errors are less than 1% of the apparent resistivities, increasing in late times to 103% for the latest time (the average error for the data is 3.2%). In contrast, the S503 sounding has a homogeneous error distribution of 11.9%. The third factor is the different physical processes inherent in the two methods, i.e., electromagnetic induction for TEM and direct current conduction for VES. This results in different sensitivities to different parameters.

The effect of varying the data redundancy is examined in Figures 9b and 9c, where the same model assessment procedure is applied to both models by varying the number of sounding data. For the T67 sounding the number was reduced to 8 equally-spaced points in the log-time scale and considering their original data errors. For the VES sounding we increased to 60 the number of data by calculating synthetic values at intermediate electrode spacings (from 20 to 3000 m of AB/2) and assigning the same original error of 11.9% to each apparent resistivity value.

The main effect of reducing the data redundancy in the T67 case is an increase in the standard errors of the seven linear combinations (Figure 9b) as compared to those with the original 60 data (Figure 8d). In particular, the standard error in the seventh row (associated with ρ_4) increased to 4450%, which reflects the large error of 1600% in this resistivity (Figure 9c). This result is the effect of having eliminated several data points containing useful information on this parameter. The increase in the number of data for S503 reduced approximately by half the standard errors in the linear combinations (compare Figure 9b with Figure 8d), with the exception of that of the seventh row, which increased to a value of 8852%, i.e., the resolution in the conductance of the third layer improved but not its resistance. The error parameters of Figure 9c for S503 display a significant improvement but still the large errors in t_3 and ρ_3 show that the increase in data redundancy did not solve the equivalence problem.

The effect of varying the data errors is shown in Figure 10. In order to compare the models in equivalent conditions, we used 8 logarithmically-spaced data with 1% data errors in both soundings. In the assessment process the data errors are included in the normalization of the coefficients of the sensitivity matrix. Smaller data errors produce larger coefficients which, after de SVD process, yield larger eigenvalues, which in turn give smaller standard errors in the different eigenparameters. The original data errors in the T67 model are less than 1% for early and intermediate times, and larger than 1% for late times. Then, the use of a uniform 1% error increases the coefficients of the sensitivity matrix associated with late times and decreases them for all other times. This explains why the errors in the shallow parameters of T67 increase (Figure 10b) with respect to those of Figure 9c, but the errors of the deeper parameters decrease.

For the S503 model, the use of 1% data errors is an improvement in the data statistics with respect to the original errors of 11.9%. The standard errors of Figure 10a show a significant improvement (with the exception of the seventh row) with respect to those of Figure 8d, even when the latter were obtained with 17 data. The importance of the data errors in the resolution of the model is seen in Figure 10b, where all the parameters show smaller errors compared to those of Figure 9a. However, the equivalence in the third layer remains, showing that this problem is not a function of the data statistics but is due to the physics of the direct current conduction.

These two tests (data redundancy and data errors) justify the very small error parameters of Figure 9a, where the T67 model shows a superior resolution because it does not suffer from any S-equivalence and the model is derived from more and better data. However, the reported parameter uncertainties should be considered as an optimistic estimate of the actual uncertainties because they were determined assuming a 1-D structure under each site. The sections of Figures 5 and 6 show that, although the gross structure is 1-D, significant lateral variations in resistivity exist in some areas, indicating the presence of 3-D effects. A particular advantage of the application of the TEM method in geothermal and hydrological problems is the common occurrence of conductive targets in these environments that may produce equivalence problems in the VES method. The reason for the good correlation between the different interfaces of T67 and S503 (Figure 8b), even though the VES model suffers from a strong equivalence problem, is the interpretation procedure adopted for the Tres Vírgenes data set, in which some of the initial models used for the VES data inversions were based on the interfaces determined from nearby TEM soundings.

The uncertainties in the VES data arise from vertical shifts between the various apparent resistivity segments. They are produced by distortions of the electric field due to the presence of near-surface inhomogeneities and topographic relief, i.e., they are of a geologic nature. As for near-surface inhomogeneities, they depend on the location and distance of the electrodes to these inhomogeneities and on their resistivity contrasts with the host rock. On the other hand, the data errors in the TEM soundings arise from electromagnetic noise produced by thunderstorms. With the exception of late times, the data errors are very small due to a large signal-to-noise-ratio resulting from stacking the decay voltages hun-

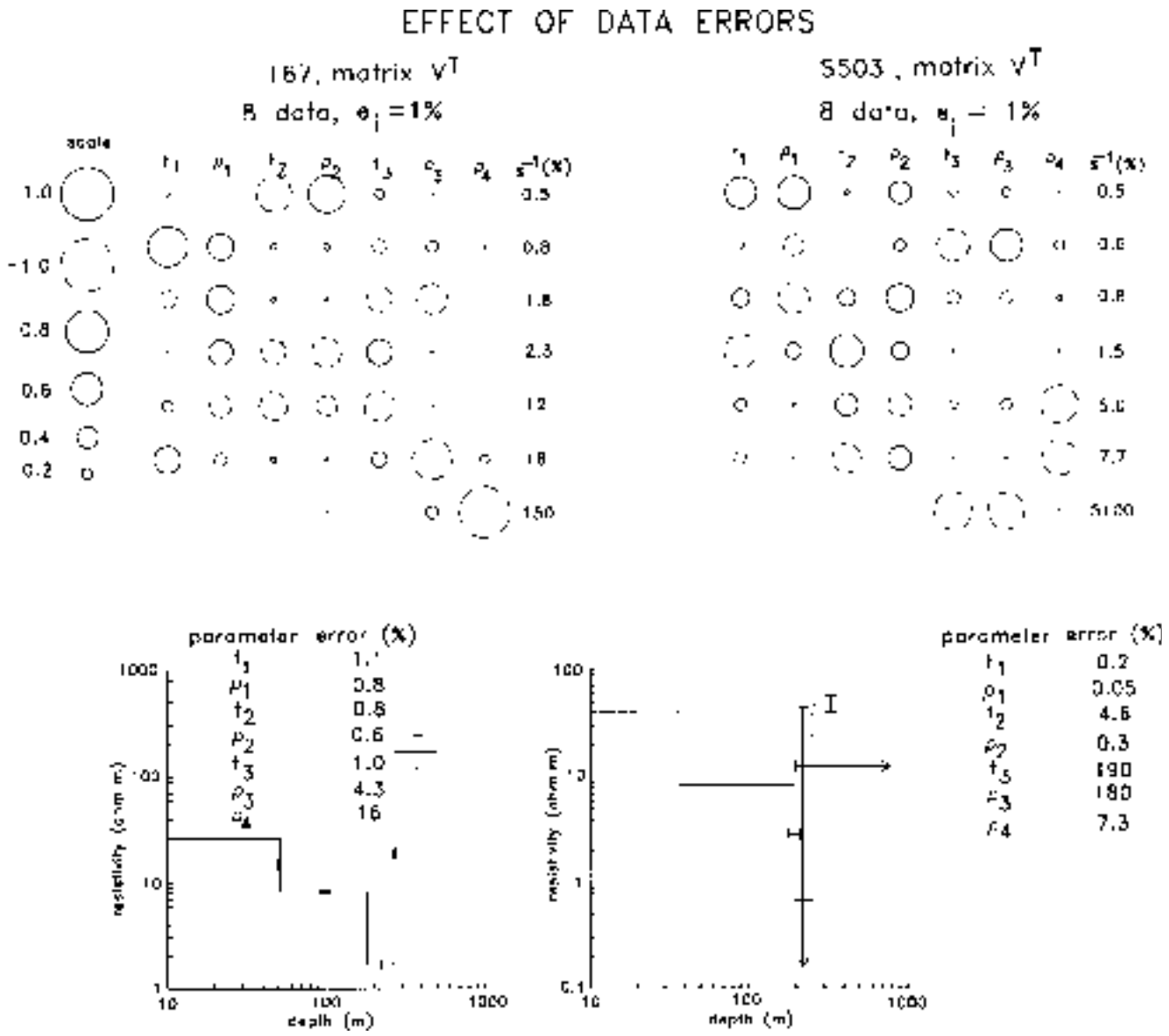

Fig. 10. Effect of varying the data errors for the Comparative Case. Both soundings consider 8 data and 1% data errors. a) Transposed eigenparameter matrices. b) Models and parameter errors.

dreds of times. Geologic noise also affects the TEM measurements but it cannot be evaluated because the transmitting loop and the receiving coil remain fixed in a sounding. In this sense, the two methods are not being compared under equal conditions because the major source of noise, of geologic type, is explicitly included in the VES data but not in the TEM measurements. However, this noise in the TEM data is expected to be less intense for several reasons. First, the magnetic field is less distorted by inhomogeneities than the electric field (Sternberg *et al*., 1988); the TEM method is based on the measurement of the time derivative of the magnetic field while the resistivity technique is based on the electric field. Second, the VES data depend on the orientation of the bipoles with respect to the strike of the underlying geology or superficial topography, while the TEM in-loop soundings integrate data over all directions, smoothing the effects from lateral variations. Third, the TEM response of a shallow 3-D body does not persist to arbitrarily late times, but it is contained within an early-time band (Pellerin and Hohmann, 1990). Thus, the deep model parameters are not significantly biased by the perturbing effect of the anomalous body. The opposite situation occurs with any EM method based on the measurement of the electric field. The presence of a surficial 3-D body not only manifests in early times (or the equivalent high frequencies) but also affects the late time (or low frequency) response. The VES technique can be considered as an EM method of zero frequency. Finally, the large electrode spreads in the Schlumberger soundings (up to 6 km of

AB) span differences in altitude of up to 400 m with a consequent major influence of topographic effects, while the array spread considered in the TEM transmitting loop is only of 150 m.

CONCLUSIONS

Using the inversion of 62 VES and 55 TEM soundings and the use of equivalent parameters, we have shown that both methods yield similar models of the subsurface. However, the TEM method offers several advantages over the VES technique. Comparable depths of penetration were reached by both methods, but the TEM soundings were obtained with 150 m square loops while the Schlumberger soundings required current electrode separations (AB/2) of 3 km. This translates into a more efficient field operation, both in time and physical effort, for the in-loop TEM technique. Model assessment shows that the TEM method has a higher resolving power. Contributing factors to this superior performance are a higher amount of information (more data and higher data density), a better quality of this information (smaller data errors and smoother observed curves), less sensitivity to perturbing effects associated with topographic relief and near-surface inhomogeneities, and less non-uniqueness in the case of S-equivalence problems. In other geologic environments, characterized by smoother topography and more uniform shallow resistivities, the superiority of the TEM technique may not be as clear as in this geothermal zone.

ACKNOWLEDGEMENTS

We are grateful for the valuable assistance of our colleagues J. M. Romo, R. Vázquez, F. Uribe, A. López, S. Espinosa, H. Benítez and R. Vega during the field acquisition campaign. We thank Dr. G. Hiriart of the Gerencia de Proyectos Geotermoeléctricos, CFE, for granting permission to publish this work, and to S. Venegas and F. Arellano for their help and useful discussions.

BIBLIOGRAPHY

ANDERSON, W. L., 1975. Improved digital filters for evaluating Fourier and Hankel transform integrals. U.S. Geol. Surv. rep. GD-75-012.

ANDERSON, W. L., 1979. Numerical integration of related Hankel transforms of orders 0 and 1 by adaptive digital filtering. *Geophysics*, 44, 1287-1305.

BALLINA, H. R. and F. HERRERA, 1985. Estudios geofísicos en la zona geotérmica de Tres Vírgenes, B.C.S. Internal report 20/84, Gerencia de Proyectos Geotermoeléctricos, CFE, 28 pp.

BIGURRA, E., 1989. Integración de estudios, Tres Vírgenes, B.C.S. Internal report 8/89, Gerencia de Proyectos Geotermoeléctricos, CFE, 28 pp.

EDWARDS, R. N., R. C. BAILEY and G. D. GARLAND, 1981. Conductivity anomalies: lower crust or asthenosphere ? *Phys. of the Earth and Planetary Ints*., 25, 263-272.

FITTERMAN, D. V. and W. L. ANDERSON, 1987. Effect of transmitter turn-off time on transient soundings. *Geoexpl.*, 24, 131-146.

FITTERMAN, D. V., J. A. C. MEEKES and I. L. RITSEMA, 1988. Equivalence behavior of three electrical sounding methods as applied to hydrogeological problems. 50th Annual Meeting of the European Ass. of Exploration Geophysicists, The Hague, the Netherlands.

FITTERMAN, D. V., 1989. Detectability levels for central induction transient soundings. *Geophysics*, 54, 127-129.

FRISCHKNECHT, F. C. and P. V. RAAB, 1984. Time-domain electromagnetic soundings at the Nevada Test Site, Nevada. *Geophysic*s, 49, 981-992.

HOVERSTEN, G. M. and H. F. MORRISON, 1982. Transient fields of a current loop source above a layered earth. *Geophysics*, 47, 1068-1077.

INMAN, J. R., 1975. Resistivity inversion with ridge regression. *Geophysics*, 40, 798-817.

JIRACEK, G. R., 1990. Near-surface and topographic distortions in electromagnetic induction. *Surveys in Geophysics*, 11, 163-203.

JONES, A. G., 1983. The problem of current channelling: A critical review. *Geophys. Surv.*, 6, 79-122.

JUPP, D. L. B. and K. VOZOFF, 1975. Stable iterative methods for the inversion of geophysical data. *Geophys. J. R. Astr. Soc.*, 42, 957-976.

KAUFMAN, A. A. and G. V. KELLER, 1983. Frequency and transient soundings: Methods in Geochemistry and Geophysics, 16, Elsevier, Amsterdam, 685 pp.

LOPEZ HERNANDEZ, A., G. GARCIA ESTRADA and F. ARELLANO GUADARRAMA, 1994. Geological and geophysical studies at Las Tres Virgenes, B.C.S., Mexico, geothermal zone. *Geotherm. Res. Counc. Trans.*, 18, 275-280.

LOPEZ HERNANDEZ, A., G. GARCIA ESTRADA and F. J. ARELLANO GUADARRAMA, 1995. Geothermal ex-

ploration at Las Tres VIirgenes, B.C.S., Mexico. *In:* Barbier, E. *et al*., eds. Proceedings of the 1995 World Geoth. Congress, Int. Geoth. Assoc., 2, 707-712.

NABIGHIAN, M. N., 1979. Quasi-static transient response of a conductive half-space - An approximate representation. *Geophysics*, 44, 1700-1705.

NABIGHIAN, M. N. and J. C. MACNAE, 1991. Time domain electromagnetic prospecting methods. *In:* Nabighian, M.N., ed. Electromagnetic methods in applied geophysics, 2, Applications, Part A, 427-479, Soc. Explor. Geophys.

ORELLANA, E. and H. M. MOONEY, 1966. Master tables and curves for vertical electrical soundings, Interciencia, Madrid.

PELLERIN, L. and G. W. HOHMANN, 1990. Transient electromagnetic inversion: A remedy for magnetotelluric static shifts. *Geophysics*, 55, 1242-1250.

RAICHE, A. P., D. L. B. JUPP, H. RUTTER and K. VOZOFF, 1985. The joint use of coincident loop transient electromagnetic and Schlumberger sounding to resolve layered structures. *Geophysics*, 50, 1618-1627.

ROMO, J. M., R. VAZQUEZ, R. VEGA, C. FLORES and A. LOPEZ, 1994. Informe de interpretación: Estudio magnetotelúrico en el área geotérmica Tres Vírgenes - El Aguajito, B.C.S., Technical Report, Contract CLS-GPG-003-94/CFE-CICESE, Gerencia de Proyectos Geotermoeléctricos.

SMITH, R. S. and G. F. WEST, 1989. Field examples of negative coincident-loop transient electromagnetic responses modeled with polarizable half-planes. *Geophysics*, 54, 1491-1498.

SPIES, B. R., 1989. Depth of investigation in electromagnetic sounding methods. *Geophysics*, 54, 872-888.

SPIES, B. R. and F. C. FRISCHKNECHT, 1991. Electromagnetic sounding. *In:* Nabighian, M.N., ed. Electr. Meth. Appl. Geophys., 2, Applications, Part A, 285-386, Soc. Explor. Geophys.

STERNBERG, B.K., J.C. WASHBURNE and L. PELLERIN, 1988. Correction for the static shift in magnetotellurics using transient electromagnetic soundings. *Geophysics*, 53, 1459-1468.

STOYER, C. H., 1990. Efficient computation of transient sounding curves for wire segments of finite length using an equivalent dipole approximation. *Geophys. Prosp*., 38, 87-100.

VAZQUEZ, R., R. VEGA, F. HERRERA and A. LOPEZ, 1992. Evaluación con métodos electromagnéticos del campo geotérmico de Tres Vírgenes, B.C.S., Primera etapa, Technical Report, Contract CLS-GPG-003-94/CFE-CICESE, Gerencia de Proyectos Geotermoeléctricos, 177 pp.

Carlos Flores[1] and Néctor Velasco[1,2]

[1] Depto. de Geofísica Aplicada. División de Ciencias de la Tierra. Centro de Investigación Científica y Educación Superior de Ensenada. Km. 107, Carretera Tijuana-Ensenada, Baja California 22830, México.

[2] Now at: Intituto Mexicano del Petróleo. Calle 56x31, Cd. del Carmen, 24180 Campeche, México.